

Nodeless superconductivity in the kagome metal CsV_3Sb_5

Weiyin Duan,^{1,2} Zhiyong Nie,^{1,2} Shuaishuai Luo,^{1,2} Fanghang Yu,³ Brenden R. Ortiz,⁴
Lichang Yin,^{1,2} Hang Su,^{1,2} Feng Du,^{1,2} An Wang,^{1,2} Ye Chen,^{1,2} Xin Lu,^{1,2} Jianjun
Ying,³ Stephen D. Wilson,⁴ Xianhui Chen,^{3,5,6} Yu Song,^{1,2,*} and Huiqiu Yuan^{1,2,6,7,†}

¹Center for Correlated Matter and Department of Physics, Zhejiang University, Hangzhou 310058, China

²Zhejiang Province Key Laboratory of Quantum Technology and Device,
Department of Physics, Zhejiang University, Hangzhou 310058, China

³Hefei National Laboratory for Physical Sciences at Microscale and Department of Physics,
and CAS Key Laboratory of Strongly-coupled Quantum Matter Physics,
University of Science and Technology of China, Hefei, Anhui 230026, China

⁴Materials Department and California Nanosystems Institute,
University of California Santa Barbara, Santa Barbara, CA, 93106, United States

⁵CAS Center for Excellence in Quantum Information and Quantum Physics, Hefei, Anhui 230026, China

⁶Collaborative Innovation Center of Advanced Microstructures, Nanjing 210093, People's Republic of China

⁷State Key Laboratory of Silicon Materials, Zhejiang University, Hangzhou 310058, China

(Dated: February 8, 2022)

The recently discovered kagome metal series AV_3Sb_5 ($A=\text{K}, \text{Rb}, \text{Cs}$) exhibits topologically non-trivial band structures, chiral charge order and superconductivity, presenting a unique platform for realizing exotic electronic states. The nature of the superconducting state and the corresponding pairing symmetry are key questions that demand experimental clarification. Here, using a technique based on the tunneling diode oscillator, the magnetic penetration depth $\Delta\lambda(T)$ of CsV_3Sb_5 was measured down to 0.07 K. A clear exponential behavior in $\Delta\lambda(T)$ with marked deviations from a T or T^2 temperature dependence is observed at low temperatures, indicating a deficiency of nodal quasiparticles. Temperature dependence of the superfluid density and electronic specific heat can be described by two-gap s -wave superconductivity, consistent with the presence of multiple Fermi surfaces in CsV_3Sb_5 . These results evidence nodeless superconductivity in CsV_3Sb_5 under ambient pressure, and constrain the allowed pairing symmetry.

PACS numbers: 74.25.Ha, 74.70.-b, 78.70.Nx

The unique geometry of the kagome lattice leads to magnetic frustration [1–3], topologically nontrivial electronic structures [4–6], and both electronic [6–8] and magnon [9] flat bands. Superconductivity with exotic pairing symmetries and properties were also predicted for the kagome lattice [10–14], although physical realizations of such exotic superconductors have been limited.

The recent discovery of superconductivity in the two-dimensional kagome metal series AV_3Sb_5 ($A = \text{K}, \text{Rb}, \text{Cs}$) provides a much-desired platform to investigate potentially exotic superconducting states on the kagome lattice [15–18]. In addition to superconductivity, these systems also exhibit a chiral charge order with unusual characteristics [19–24], topological band crossings [15, 16], and a giant anomalous Hall effect in the absence of magnetic local moments [16, 25–27]. The nature of the superconducting state in the presence of these electronic states, remains to be clarified. Nonetheless, tantalizing evidence for an unusual superconducting state has emerged from the observation of spin-triplet supercurrent in $\text{K}_{1-x}\text{V}_3\text{Sb}_5$ Josephson junctions [28] and possible Majorana bound states inside the superconducting vortex cores of CsV_3Sb_5 [29].

A hallmark of unconventional superconductivity is a sign-changing superconducting order parameter [30, 31]. While direct phase-sensitive evidence for such a sign-

change is difficult to obtain [32, 33], for a number of pairing symmetries the sign-change mandates nodes in the superconducting order parameter (such as $d_{x^2-y^2}$ -pairing in the cuprates), and can be probed through various experimental techniques. Thermal conductivity measurements on CsV_3Sb_5 down to 0.15 K indicated possible nodal quasiparticles [34], and superconducting domes were found in the temperature-pressure phase diagrams of AV_3Sb_5 [34–36], reminiscent of behaviors in established unconventional superconductors. On the other hand, the tunneling spectrum of CsV_3Sb_5 measured by scanning tunneling microscopy could be described by an anisotropic s -wave gap without nodes [29]. To further clarify the pairing symmetry in the AV_3Sb_5 series, experiments sensitive to low-energy excitations are badly needed.

In this work, the magnetic penetration depth and specific heat of the kagome metal CsV_3Sb_5 were measured to probe its superconducting gap structure. The change of the magnetic penetration depth reveals a clear exponential behavior down to 0.07 K, and deviates significantly from a T or T^2 temperature dependence. Such a behavior suggests an absence of nodal quasiparticles, and instead points to fully-gapped superconductivity in CsV_3Sb_5 under ambient pressure. By analyzing the derived superfluid density and electronic specific heat, a two-gap s -

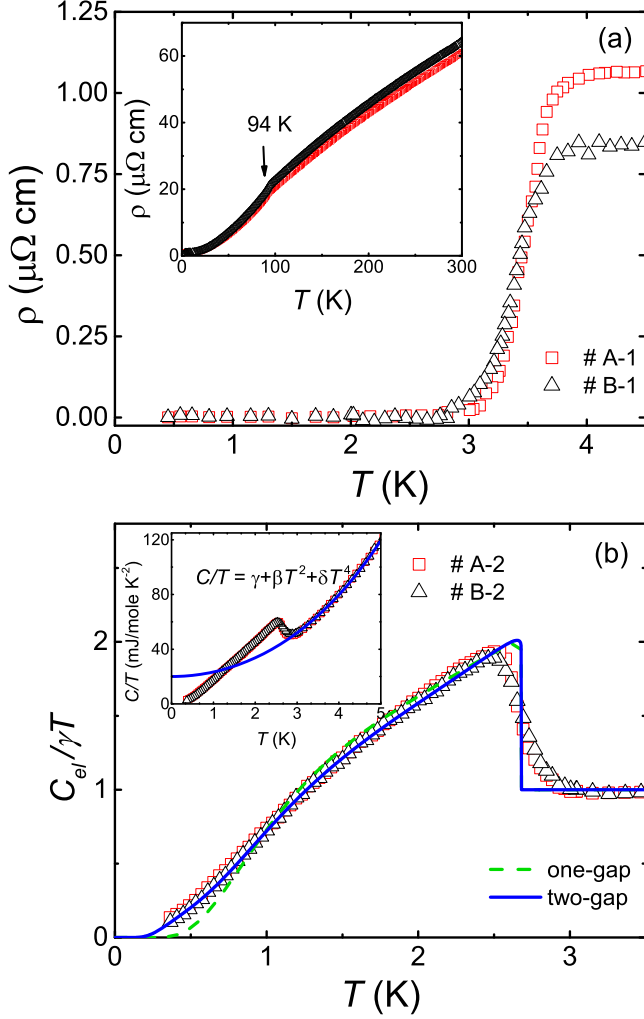


Figure 1: (Color online) Temperature dependence of the low temperature (a) resistivity $\rho(T)$ and (b) electronic specific heat $C_{el}(T)/\gamma T$ for CsV_3Sb_5 . The inset in (a) shows $\rho(T)$ from 0.45 K up to 300 K. The inset in (b) shows the specific heat $C(T)/T$, with the blue solid line being a fit to the normal state specific heat, including contributions from electrons and phonons. The solid and dashed lines in (b) are fits to a single-gap and two-gap s -wave superconducting model, respectively.

wave superconducting order parameter is found to capture the experimental data. These results provide evidence for nodeless superconductivity in CsV_3Sb_5 under ambient pressure, and rule out pairing with symmetry-enforced nodes.

Single crystals of CsV_3Sb_5 were synthesized using the self-flux method, at the University of Science and Technology of China (sample A) and the University of California, Santa Barbara (sample B), with physical properties separately characterized and described in previous works [16, 27]. Eight samples were examined with various approaches, and are labeled samples #A-1 to #A-5, and samples #B-1 to #B-3. The ab -plane electrical resistivity $\rho(T)$ was measured in a ^3He cryostat, using a standard four-probe method. Specific heat was measured using a

Quantum Design Physical Property Measurement System (PPMS) with a ^3He insert, using a standard pulse relaxation method. The change in the London penetration depth $\Delta\lambda(T) = \lambda(T) - \lambda(0)$ was measured using a tunnel diode oscillator (TDO) [37, 38], with an operating frequency of about 7 MHz. The TDO method can precisely measure the temperature dependence of the magnetic penetration depth change, offering a powerful probe of low-energy excitations in the superconducting state. TDO measurements down to 0.35 K and 0.07 K, with noise levels as low as 0.1 Hz and 0.5 Hz, were carried out in ^3He and dilution refrigerators, respectively. The ac field generated by the coil (20 mOe) is far below the lower critical field H_{c1} of CsV_3Sb_5 , ensuring that the sample remains in the full Meissner state throughout the measurements. $\Delta\lambda(T)$ can be obtained from the frequency shift $\Delta f(T)$ of the TDO through $\Delta\lambda(T) = G\Delta f(T)$, where G is a sample-dependent scale factor [39].

The inset of Fig. 1(a) shows the electrical resistivity $\rho(T)$ of CsV_3Sb_5 from 300 K down to 0.45 K. A clear kink can be observed around 94 K, due to the onset of charge order [15, 16]. The temperature evolution of $\rho(T)$ for samples #A-1 and #B-1 are highly similar, with residual resistivity ratios (RRR) of ≈ 57 and ≈ 74 , respectively. Fig. 1(a) zooms into $\rho(T)$ below 4.5 K, where a clear superconducting transition can be observed, which onsets around 3.5 K and zero resistance appears below ≈ 2.7 K in both samples. The residual resistivities just above the onset of superconductivity are also similar, close to $1 \mu\Omega \text{ cm}$ in both samples. Measurements of the low temperature specific heat $C(T)/T$ are shown in the inset of Fig. 1(b) for samples #A-2 and #B-2, demonstrating the appearance of bulk superconductivity below $T_c \approx 2.7$ K. In the normal state, the specific heat can be modeled using $C(T)/T = \gamma + \beta T^2 + \delta T^4$, with $\gamma = 20.03 \text{ mJ mole}^{-1} \text{ K}^{-2}$, $\beta = 3.306 \text{ mJ mole}^{-1} \text{ K}^{-4}$ and $\delta = 26.78 \mu\text{J mole}^{-1} \text{ K}^{-6}$ (solid line in the inset of Fig. 1(b)). Here γ is the Sommerfeld coefficient, and the other two parameters characterize the contribution from phonons. After subtracting the phonon contribution, the electronic specific heat $C_{el}(T)/\gamma T$ can be obtained, shown in Fig. 1(b). Analysis of $C_{el}(T)/\gamma T$ will be further discussed below. Combining the coherence length ξ ($\approx 26 \text{ nm}$ from $H_{c2} = 0.47 \text{ T}$ [16, 27]), residual resistivity ρ_0 , and the Sommerfeld coefficient γ , mean free paths of 680 nm and 830 nm are estimated [40, 41] for samples #A-1 and #B-1, respectively. These values are much larger than the coherence length, indicating that the samples are in the clean limit. Our resistivity and specific heat results are consistent with previous reports [16, 27], and indicate samples A and B are similar and that both are of high quality.

Fig. 2 shows the temperature dependence of the magnetic penetration depth for CsV_3Sb_5 . Three samples were studied with applied field along the c -axis, with $G = 7.8 \text{ \AA/Hz}$, 9.1 \AA/Hz and 9.8 \AA/Hz , for samples

#A-3, #A-4 and #B-3, respectively. Sample #A-5 was studied with field perpendicular to the c -axis, with its $\Delta\lambda(T)$ scaled to that of sample #A-3, due to difficulties in accurately determining the G factor for a thin sample. The inset in Fig. 2(a) shows $\Delta\lambda(T)$ for samples #A-3 and #A-5 from 4.5 K down to 0.07 K, exhibiting clear reductions upon cooling due to superconductivity, consistent with resistivity and specific heat measurements in Fig. 1. $\Delta\lambda(T)$ with applied field along and perpendicular to the c -axis are compared in Fig. 2(a) for samples #A-3 and #A-5, revealing almost identical behaviors, suggesting that the superconducting state is rather isotropic. Fig. 2(b) compares the low temperature penetration depth $\Delta\lambda(T)$ for three CsV₃Sb₅ samples with field applied along the c -axis. The data for different samples almost overlap, confirming the superconducting properties of samples A and B are similar, and demonstrate that our results are reproducible and reflect the intrinsic behavior of CsV₃Sb₅.

For a nodal superconductor in the clean limit, it is expected that the magnetic penetration depth exhibits a power-law behavior in the low temperature limit, *i.e.*, $\Delta\lambda \sim T^n$, with $n = 1$ and 2 respectively corresponding to line nodes and point nodes being present in the gap structure. From Fig. 2(b), it can be seen that the experimentally measured $\Delta\lambda(T)$ obviously deviates from a T or T^2 behavior, but is reasonably described by $\Delta\lambda(T) \sim T^{2.9}$ with a slight deviation at low temperatures. To further analyze the power law dependence of $\Delta\lambda(T)$, the experimental data is fit by $\Delta\lambda(T) \sim T^n$ from 0.07 K to various temperatures, with the best fit n shown in the inset of Fig. 2(b). It can be seen that the exponent $n \approx 3$ appears for $T > 0.2T_c$, and becomes significantly enhanced at lower temperatures. Such a power law behavior ($n \gtrsim 3$), in particular the progressive increase of n with decreasing temperature, is consistent with an exponential behavior, and suggests an absence of gap nodes in the superconducting state of CsV₃Sb₅.

To further analyze the magnetic penetration depth, $\Delta\lambda(T)$ is fit to an s -wave gap at low temperatures, with

$$\Delta\lambda(T) \sim T^{-\frac{1}{2}} \exp\left(-\frac{\Delta(0)}{k_B T}\right), \quad (1)$$

where $\Delta(0)$ is the gap value at zero temperature. It can be seen that such an s -wave model fits the experimental data well at low temperatures, providing strong evidence for nodeless superconductivity in CsV₃Sb₅. The derived small superconducting gap of $\Delta(0) = 0.59 k_B T_c$ indicates that $\Delta\lambda(T)$ would only saturate at very low temperatures, as seen in Fig. 2(b), and a multi-gap model is needed in order to describe $\Delta\lambda(T)$.

To further extract information about the superconducting state, the normalized superfluid density is obtained through $\rho_s(T) = [\lambda(0)/\lambda(T)]^2$. The value of the zero-temperature penetration depth $\lambda(0) = 387$ nm was estimated using $\lambda(0) = \sqrt{\phi_0 H_{c2}(0)/\sqrt{24}\gamma\Delta(0)}$ [42],

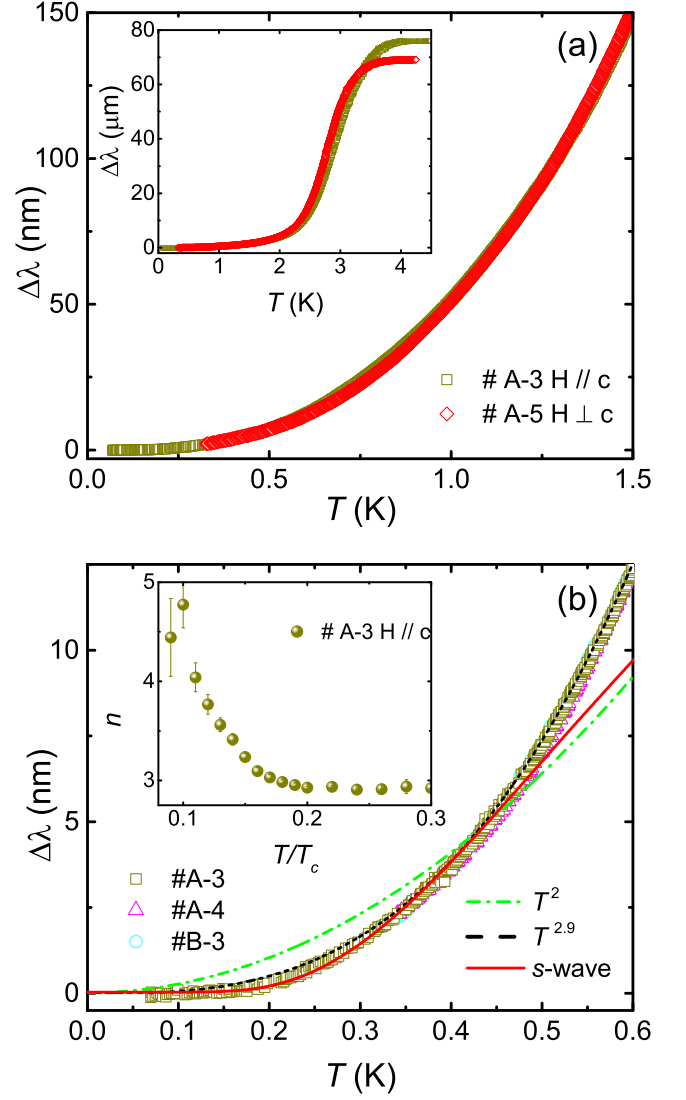


Figure 2: (Color online) (a) Comparison of $\Delta\lambda(T)$ for applied fields along and perpendicular to the c -axis. The inset shows $\Delta\lambda(T)$ from 4.5 K down to 0.07 K. (b) The change of the penetration depth $\Delta\lambda(T)$, measured for three CsV₃Sb₅ samples with field along the c -axis. The dash-dotted and dashed lines respectively represent fits using a T^2 and a T^n temperature dependence, from 0.07 K up to 0.6 K. The solid lines represent a fit to Eq. 1. The inset shows the exponent n , obtained by fitting $\Delta\lambda(T)$ to a T^n behavior from 0.07 K up to different temperatures of T/T_c .

where ϕ_0 is the magnetic-flux quantum, the Sommerfeld coefficient γ is obtained from specific heat measurements (inset of Fig. 1(b)), $H_{c2}(0) = 0.47$ T [16, 27] and the weak-coupling limit of BCS theory with $\Delta(0) = 1.76 k_B T_c$ is assumed. ρ_s obtained this way is shown as a function of the reduced temperature T/T_c for sample #A-3 in Fig. 3(a), and is fit to several different models of the superconducting gap function Δ_k , which is related to ρ_s through

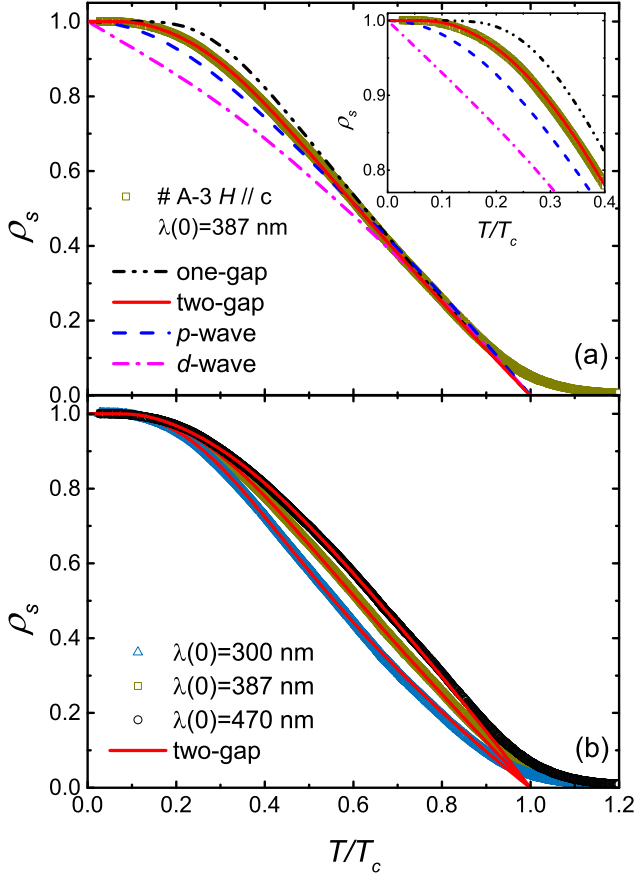


Figure 3: (Color online) Normalized superfluid density ρ_s for sample #A-3 with $\lambda(0) = 387$ nm, as a function of the reduced temperature T/T_c . The dash-dot-dotted, solid, dashed, and dash-dotted lines respectively represent fits to models with a single s -wave gap, two s -wave gaps, a p -wave gap, and a d -wave gap. The inset zooms into the low temperature region of the figure. (b) Comparison of ρ_s for different values of $\lambda(0)$. The solid lines are fits to a two-gap s -wave model.

$$\rho_s(T) = 1 + 2 \left\langle \int_{\Delta_k}^{\infty} \frac{E dE}{\sqrt{E^2 - \Delta_k^2}} \frac{\partial f}{\partial E} \right\rangle_{\text{FS}}, \quad (2)$$

where $f(E, T) = [1 + \exp(\frac{E}{k_B T})]^{-1}$ is the Fermi-Dirac distribution, and $\langle \dots \rangle_{\text{FS}}$ represents averaging over the Fermi surface. Temperature dependence of the superconducting order parameter is approximated using

$$\Delta(T) = \Delta(0) \tanh \left\{ 1.82 [1.018 (T_c/T - 1)]^{0.51} \right\}. \quad (3)$$

As can be seen, the data are clearly incompatible with a single-gap s -wave model, a p -wave model with point nodes, and a d -wave model with line nodes. These models exhibit significant deviations from the data, especially at low temperatures (inset of Fig. 3(a)). On the other hand, a two-gap s -wave model describes the data well over the entire temperature range (solid line in Fig. 3(a)). The fit

gap values are $\Delta_1(0) = 1.42 k_B T_c$ and $\Delta_2(0) = 0.58 k_B T_c$, with weights of the two gaps being 87% and 13%, respectively. The deduced small gap of $\Delta_2 = 0.58 k_B T_c$ is consistent with $\Delta = 0.59 k_B T_c$ derived from fitting $\Delta\lambda(T)$ at low-temperature (Fig. 2(b)). Considering possible uncertainties in the estimate of $\lambda(0)$ and to test the robustness of our conclusions, $\lambda(0)$ is varied by $\approx \pm 20\%$ from 387 nm and the analyses are repeated, with results shown in Fig. 3(b). It is found that the two-gap s -wave model describes ρ_s well in all cases (solid lines), while other models in Fig. 3(a) exhibit clear deviations. For $\lambda(0) = 300$ nm, $\Delta_1(0) = 1.23 k_B T_c$ and $\Delta_2(0) = 0.50 k_B T_c$ are obtained, while $\Delta_1(0) = 1.63 k_B T_c$ and $\Delta_2(0) = 0.66 k_B T_c$ are obtained for $\lambda(0) = 470$ nm. Our analyses of the superfluid density therefore support the idea that CsV_3Sb_5 exhibits multiband nodeless superconductivity. It is noted that the larger gap $\Delta_1(0)$ is close to but still smaller than the BCS value of $1.76 k_B T_c$, the origin of which is not clear. It is possible that the contribution of an additional band or the effect of an anisotropic gap may lead to such a weak deviation.

To confirm the above conclusion, the low temperature electronic specific heat $C_{\text{el}}(T)/\gamma T$ of CsV_3Sb_5 is analyzed, shown in Fig. 1(b). Similar to the superfluid density, it is found that a single s -wave gap does not capture the behavior of $C_{\text{el}}(T)/\gamma T$ (solid line in Fig. 1(b)), while a two-gap s -wave model gives an excellent description of the experimental data over the full temperature range (dashed line in Fig. 1(b)). The fit gap values are $\Delta_1(0) = 1.62 k_B T_c$ and $\Delta_2(0) = 0.63 k_B T_c$, with weights of 79% and 21%, respectively. These values are in reasonable agreement with analysis of the superfluid density, and supports the notion that CsV_3Sb_5 exhibits fully-gapped multiband superconductivity.

The low temperature exponential behavior of $\Delta\lambda(T)$ provides evidence for nodeless superconductivity, while the extracted small gap and analysis of both the superfluid density and the electronic specific heat evidence multiband superconductivity. This is consistent with the presence of multiple Fermi surfaces revealed by angle-resolved photoemission spectroscopy measurements and electronic structure calculations [16]. Such a picture is supported by the consideration that the pocket around Γ and the Fermi surfaces around M are mainly associated with Sb p_z and V d orbitals, respectively [24], and are likely associated with superconducting gaps of different sizes. It should be noted that our analyses do not exclude an anisotropic s -wave superconducting gap. However, considering that this is a multiband system, and the penetration depth along different directions are similar (Fig. 2(a)), multi-gap superconductivity appears more likely.

Since a circular Fermi surface around Γ is present in CsV_3Sb_5 [16], all even-parity basis gap functions associated with the D_{6h} point group would lead to symmetry-enforced nodes, except that of the A_{1g} channel [43].

Therefore, the finding of nodeless superconductivity indicates the pairing symmetry of CsV_3Sb_5 belongs to the even-parity A_{1g} representation, or odd-parity nodeless representations. While our results can be described by a superconducting state with two s -wave gaps, and is supported by the presence of multiple Fermi surfaces in CsV_3Sb_5 , our measurements do not rule out some exotic unconventional superconducting states. These include spin-triplet nodeless superconductivity [44], s^\pm -pairing as in the iron-based superconductors [45], and pairing with band-mixing as suggested for CeCu_2Si_2 [46].

Upon pressure-tuning, superconductivity in CsV_3Sb_5 exhibits significant modulations and exhibit at least two superconducting domes [34, 35], suggesting the presence of competing superconducting ground states. As our results evidence a nodeless superconducting state under ambient pressure, whether the competing superconducting state stabilized under pressure remains nodeless or exhibits symmetry-enforced nodes, becomes an important question to be addressed in future works.

In conclusion, the superconducting pairing symmetry of CsV_3Sb_5 single crystals is probed through magnetic penetration depth measurements down to 0.07 K. A clear exponential behavior at low temperatures provides evidence for nodeless superconductivity in CsV_3Sb_5 under ambient pressure. Temperature dependence of the superfluid density and electronic specific heat can be described by two-gap s -wave superconductivity, consistent with the presence of multiple Fermi surfaces in CsV_3Sb_5 . Our results are inconsistent with pairing with symmetry-enforced nodes in CsV_3Sb_5 , but do not rule out fully-gapped unconventional superconductivity.

This work was supported by the National Key R&D Program of China (No. 2017YFA0303100, No. 2016YFA0300202), the Key R&D Program of Zhejiang Province, China (2021C01002), the National Natural Science Foundation of China (No. 11974306 and No. 12034017). S.D.W. and B.R.O. gratefully acknowledge support via the UC Santa Barbara NSF Quantum Foundry funded via the Q-AMASE-i program under award DMR-1906325. B.R.O. also acknowledges support from the California NanoSystems Institute through the Elings fellowship program.

* Electronic address: yusong.phys@zju.edu.cn

† Electronic address: hqyuan@zju.edu.cn

- [1] I. Syozi, Progress of Theoretical Physics **6**, 306 (1951), URL <https://doi.org/10.1143/ptp/6.3.306>.
- [2] T.-H. Han, J. S. Helton, S. Chu, D. G. Nocera, J. A. Rodriguez-Rivera, C. Broholm, and Y. S. Lee, Nature **492**, 406 (2012), URL <https://doi.org/10.1038/nature11659>.
- [3] C. Broholm, R. J. Cava, S. A. Kivelson, D. G. Nocera, M. R. Norman, and T. Senthil, Science **367**, eaay0668 (2020), URL <https://doi.org/10.1126/science.aay0668>.
- [4] L. Ye, M. Kang, J. Liu, F. von Cube, C. R. Wicker, T. Suzuki, C. Jozwiak, A. Bostwick, E. Rotenberg, D. C. Bell, et al., Nature **555**, 638 (2018), URL <https://doi.org/10.1038/nature25987>.
- [5] E. Liu, Y. Sun, N. Kumar, L. Muechler, A. Sun, L. Jiao, S.-Y. Yang, D. Liu, A. Liang, Q. Xu, et al., Nature Physics **14**, 1125 (2018), URL <https://doi.org/10.1038/s41567-018-0234-5>.
- [6] M. Kang, L. Ye, S. Fang, J.-S. You, A. Levitan, M. Han, J. I. Facio, C. Jozwiak, A. Bostwick, E. Rotenberg, et al., Nature Materials **19**, 163 (2019), URL <https://doi.org/10.1038/s41563-019-0531-0>.
- [7] Z. Lin, J.-H. Choi, Q. Zhang, W. Qin, S. Yi, P. Wang, L. Li, Y. Wang, H. Zhang, Z. Sun, et al., Physical Review Letters **121** (2018), URL <https://doi.org/10.1103/physrevlett.121.096401>.
- [8] J.-X. Yin, S. S. Zhang, G. Chang, Q. Wang, S. S. Tsirkin, Z. Guguchia, B. Lian, H. Zhou, K. Jiang, I. Belopolski, et al., Nature Physics **15**, 443 (2019), URL <https://doi.org/10.1038/s41567-019-0426-7>.
- [9] R. Chisnell, J. Helton, D. Freedman, D. Singh, R. Bewley, D. Nocera, and Y. Lee, Physical Review Letters **115** (2015), URL <https://doi.org/10.1103/physrevlett.115.147201>.
- [10] W.-H. Ko, P. A. Lee, and X.-G. Wen, Physical Review B **79** (2009), URL <https://doi.org/10.1103/physrevb.79.214502>.
- [11] S.-L. Yu and J.-X. Li, Physical Review B **85** (2012), URL <https://doi.org/10.1103/physrevb.85.144402>.
- [12] W.-S. Wang, Z.-Z. Li, Y.-Y. Xiang, and Q.-H. Wang, Physical Review B **87** (2013), URL <https://doi.org/10.1103/physrevb.87.115135>.
- [13] M. L. Kiesel, C. Platt, and R. Thomale, Physical Review Letters **110** (2013), URL <https://doi.org/10.1103/physrevlett.110.126405>.
- [14] I. I. Mazin, H. O. Jeschke, F. Lechermann, H. Lee, M. Fink, R. Thomale, and R. Valentí, Nature Communications **5** (2014), URL <https://doi.org/10.1038/ncomms5261>.
- [15] B. R. Ortiz, L. C. Gomes, J. R. Morey, M. Winiarski, M. Bordelon, J. S. Mangum, I. W. H. Oswald, J. A. Rodriguez-Rivera, J. R. Neilson, S. D. Wilson, et al., Physical Review Materials **3** (2019), URL <https://doi.org/10.1103/physrevmaterials.3.094407>.
- [16] B. R. Ortiz, S. M. Teicher, Y. Hu, J. L. Zuo, P. M. Sarte, E. C. Schueller, A. M. Abeykoon, M. J. Krogstad, S. Rosenkranz, R. Osborn, et al., Physical Review Letters **125** (2020), URL <https://doi.org/10.1103/physrevlett.125.247002>.
- [17] B. R. Ortiz, E. Kenney, P. M. Sarte, S. M. L. Teicher, R. Seshadri, M. J. Graf, and S. D. Wilson (2020), arXiv:2012.09097.
- [18] Q. Yin, Z. Tu, C. Gong, Y. Fu, S. Yan, and H. Lei (2021), arXiv:2101.10193.
- [19] Y.-X. Jiang, J.-X. Yin, M. M. Denner, N. Shumiya, B. R. Ortiz, J. He, X. Liu, S. S. Zhang, G. Chang, I. Belopolski, et al. (2020), arXiv:2012.15709.
- [20] H. Zhao, H. Li, B. R. Ortiz, S. M. L. Teicher, T. Park, M. Ye, Z. Wang, L. Balents, S. D. Wilson, and I. Zeljkovic (2021), arXiv:2103.03118.
- [21] H. Chen, H. Yang, B. Hu, Z. Zhao, J. Yuan, Y. Xing, G. Qian, Z. Huang, G. Li, Y. Ye, et al. (2021),

- arXiv:2103.09188.
- [22] H. X. Li, T. T. Zhang, Y. Y. Pai, C. Marvinney, A. Said, T. Yilmaz, Q. Yin, C. Gong, Z. Tu, E. Vescovo, et al. (2021), arXiv:2103.09769.
 - [23] H. Tan, Y. Liu, Z. Wang, and B. Yan (2021), arXiv:2103.06325.
 - [24] X. Feng, K. Jiang, Z. Wang, and J. Hu (2021), arXiv:2103.07097.
 - [25] S.-Y. Yang, Y. Wang, B. R. Ortiz, D. Liu, J. Gayles, E. Derunova, R. Gonzalez-Hernandez, L. Šmejkal, Y. Chen, S. S. P. Parkin, et al., *Science Advances* **6**, eabb6003 (2020), URL <https://doi.org/10.1126/sciadv.abb6003>.
 - [26] E. M. Kenney, B. R. Ortiz, C. Wang, S. D. Wilson, and M. J. Graf (2020), arXiv:2012.04737.
 - [27] F. H. Yu, T. Wu, Z. Y. Wang, B. Lei, W. Z. Zhuo, J. J. Ying, and X. H. Chen (2021), arXiv:2102.10987.
 - [28] Y. Wang, S. Yang, P. K. Sivakumar, B. R. Ortiz, S. M. L. Teicher, H. Wu, A. K. Srivastava, C. Garg, D. Liu, S. S. P. Parkin, et al. (2020), arXiv:2012.05898.
 - [29] Z. Liang, X. Hou, W. Ma, F. Zhang, P. Wu, Z. Zhang, F. Yu, J. J. Ying, K. Jiang, L. Shan, et al. (2021), arXiv:2103.04760.
 - [30] D. J. Scalapino, *Reviews of Modern Physics* **84**, 1383 (2012), URL <https://doi.org/10.1103/revmodphys.84.1383>.
 - [31] G. R. Stewart, *Advances in Physics* **66**, 75 (2017), URL <https://doi.org/10.1080/00018732.2017.1331615>.
 - [32] D. J. V. Harlingen, *Reviews of Modern Physics* **67**, 515 (1995), URL <https://doi.org/10.1103/revmodphys.67.515>.
 - [33] C. C. Tsuei and J. R. Kirtley, *Reviews of Modern Physics* **72**, 969 (2000), URL <https://doi.org/10.1103/revmodphys.72.969>.
 - [34] C. C. Zhao, L. S. Wang, W. Xia, Q. W. Yin, J. M. Ni, Y. Y. Huang, C. P. Tu, Z. C. Tao, Z. J. Tu, C. S. Gong, et al. (2021), arXiv:2102.08356.
 - [35] K. Y. Chen, N. N. Wang, Q. W. Yin, Z. J. Tu, C. S. Gong, J. P. Sun, H. C. Lei, Y. Uwatoko, and J. G. Cheng (2021), arXiv:2102.09328.
 - [36] F. Du, S. Luo, B. R. Ortiz, Y. Chen, W. Duan, D. Zhang, X. Lu, S. D. Wilson, Y. Song, and H. Yuan (2021), 2102.10959.
 - [37] C. T. Van Degrift, *Rev. Sci. Instrum.* **46**, 599 (1975), URL <https://doi.org/10.1063/1.1134272>.
 - [38] E. M. E. Chia, Ph.D. thesis, University of Illinois at UrbanaChampaign (2004), URL <http://research.physics.illinois.edu/Publications/theses/co>
 - [39] R. Prozorov, R. W. Giannetta, A. Carrington, and F. M. Araujo-Moreira, *Phys. Rev. B* **62**, 115 (2000), URL <https://link.aps.org/doi/10.1103/PhysRevB.62.115>.
 - [40] T. P. Orlando, E. J. McNiff, S. Foner, and M. R. Beasley, *Physical Review B* **19**, 4545 (1979), URL <https://doi.org/10.1103/physrevb.19.4545>.
 - [41] H. Q. Yuan, D. F. Agterberg, N. Hayashi, P. Badica, D. Vandervelde, K. Togano, M. Sigrist, and M. B. Salamon, *Physical Review Letters* **97** (2006), URL <https://doi.org/10.1103/physrevlett.97.017006>.
 - [42] F. Gross, B. S. Chandrasekhar, D. Einzel, K. Andres, P. J. Hirschfeld, H. R. Ott, J. Beuers, Z. Fisk, and J. L. Smoth, *Z. Phys. B: Condens. Matter* **64**, 175 (1986), URL <https://doi.org/10.1007/BF01303700>.
 - [43] M. Sigrist and K. Ueda, *Reviews of Modern Physics* **63**, 239 (1991), URL <https://doi.org/10.1103/revmodphys.63.239>.
 - [44] R. Balian and N. R. Werthamer, *Physical Review* **131**, 1553 (1963), URL <https://doi.org/10.1103/physrev.131.1553>.
 - [45] P. J. Hirschfeld, M. M. Korshunov, and I. I. Mazin, *Reports on Progress in Physics* **74**, 124508 (2011), URL <https://doi.org/10.1088/0034-4885/74/12/124508>.
 - [46] G. Pang, M. Smidman, J. Zhang, L. Jiao, Z. Weng, E. M. Nica, Y. Chen, W. Jiang, Y. Zhang, W. Xie, et al., *Proceedings of the National Academy of Sciences* **115**, 5343 (2018), URL <https://doi.org/10.1073/pnas.1720291115>.